Molecular doping and gas sensing in Si nanowires: From charge injection to reduced dielectric mismatch

UNIVERSITÀ DEGLI STUDI DI TORINO

G. Amato, A. Cultrera, L. Boarino, C. Lamberti, S. Bordiga, F. Mercuri, X, Cartoixà, R. Rurali "Molecular doping in Si nanowires revisited: from charge injection to reduced dielectric mismatch", *J. Appl. Phys.*, **114** (2013) Art. n. 204302. DOI: 10.1063/1.4834576

Molecular doping and gas sensing in Si nanowires: from charge injection to reduced dielectric mismatch

Giampiero Amato,[1] Alessandro Cultrera,[2] Luca Boarino,[1] Carlo Lamberti,[2]
Silvia Bordiga,[2] Francesco Mercuri,[3] Xavier Cartoixà,[4] and Riccardo Rurali[5]

[1] *Quantum Research Lab., Istituto Nazionale di Ricerca Metrologica, strada delle Cacce 91, 10135 Torino, Italy*

[2] *Department of Chemistry, NIS Centre of Excellence and INSTM Reference Center, Via Quarello 11, Università di Torino, 10135 Torino, Italy*

[3] *CNR Institute for Nanostructured Materials, via P. Gobetti 101, 40129 Bologna, Italy*

[4] *Departament d'Enginyeria Electrònica, Universitat Autònoma de Barcelona, 08193 Bellaterra (Barcelona), Spain*

[5] *Institut de Ciència de Materials de Barcelona (CSIC), Campus de Bellaterra, 08193 Bellaterra, Barcelona, Spain*[*]

(Dated: October 23, 2013)

Abstract

We report experimental and theoretical evidence of the different mechanisms that lead to doping of Si nanowires upon molecular adsorption of two paradigmatic Lewis bases. Pyridine genuinely dopes the nanowires by injecting charge carriers. Ethanol, on the other hand, simply modifies the dielectric screening conditions, allowing the reactivation of preexisting electrically passive impurities, and thus cannot control neither the nature (*n*- vs *p*-type) nor the concentration of the carriers.

[*] rrurali@icmab.es

I. INTRODUCTION

Semiconducting nanowires are attracting great interest as candidate material for a new generation of versatile electronic devices. Si nanowires (SiNWs) [1], in particular, are a very appealing solution for their ideal compatibility with the conventional, state-of-the-art Si electronics, which will still continue being the backbone of most device applications. Doping, the ability to modify the conductivity of a semiconductor, is the core of device design and it is proving to be increasingly challenging for ultra-scaled nanowires [2]. Quantum confinement [3, 4], dielectric confinement [5, 6], and surface segregation [7, 8] all concur, though through different mechanisms, to make conventional doping impurities such as B or P electrically inactive in sub-20 nm SiNWs. On top of that, it is very difficult to obtain uniform axial and radial impurity concentrations by means of *in-situ* doping during vapor-liquid-solid (VLS) growth, due to the competition between catalyzed incorporation of the dopants through the liquid droplet and uncatalyzed deposition on the sidewalls of the nanowire [9, 10].

Molecular doping, the injection of free carriers by molecule adsorption, would potentially solve most of these problems and is therefore of great interest for nanoelectronics applications [11]. Besides that, gas sensing is a topic of paramount technological importance *per se*, for instance in environmental monitoring and for the safety control of many industrial processes, and systems with a large surface-to-bulk ratio such as nanowires, and nanostructured semiconductors in general, appear to be especially attractive for this class of applications.

A few experiments of molecular doping in SiNWs have been reported recently [12–17], but a unified understanding of the underlying atomic scale doping mechanism is still lacking. In particular, the difference between direct charge injection and dielectric screening effects has not been properly outlined. This difference is not very important when it comes to sensing, as in both cases a change in the conductivity is observed. However, it becomes essential if one intends to *dope* the material, i.e. modifying the carrier concentration in a *controlled* way.

Here we present a combined experimental and theoretical study of the adsorption of Pyridine and Ethanol, as prototypes of N- and O-containing Lewis bases, in a network of SiNWs. Pyridine and ethanol have been chosen because of their different interaction with the Si nano-skeleton: the first is a reducing base capable of injecting electrons while the second is expected to be chemically inert. As we will show, the study of these two systems allows comparing directly charge injection vs. dielectric screening as a result of molecular

adsorption. To this purpose, we propose a novel and simple method based on infrared spectroscopy that gives us access to the estimated carrier concentration and the dielectric screening conditions within a single measurement.

II. EXPERIMENTAL AND THEORETICAL METHODOLOGY

Instead of stand-alone VLS-grown nanowires, we use a disordered network of nanowires (DNN) as obtained by the well-established electrochemical etching process developed for the preparation of mesoporous Si. The reason for this choice is twofold: (i) the much larger surface area gives a higher throughput in the gas sensing experiments, and (ii) the average diameter of the nanowires of the etched web is 5-12 nm [18–20], which is exactly the size range where the larger sensitivity to dielectric confinement is expected [5], a crucial fact for reasons that will be discussed below.

Mesoporous Si membranes have been prepared by electrochemical etching of p+ Si (Boron doped, conductivity of $8 - 12$ m$\Omega \cdot$ cm, $\langle 100 \rangle$ oriented), mounted in a teflon cell after the backside oxide removal. After cell filling with 25 % HF aqueous etching solution (HF[50 %] in ethanol 1:1 in water), several etching and rest cycles were performed ($J = 250$ mA/cm^2 current density for 1 s and $J = -1$ mA/cm^2 for 10 s) to improve the samples in-depth homogeneity. Then, the membranes have been detached by lowering the HF concentration of the etching solution and applying $J = 1$ A/cm^2 for 3 s.

The ~ 20 μm thick membranes, (a value outcoming from thickness measurement of the substrates by a Tencor P-10 stylus profiler) were estimated have porosity about 74 ± 2 % from calibration curves. The membranes were transferred onto p-type Si plates as support with no fractures. The as-supported membranes were enclosed in vacuum-ready Fourier transform infrared (FTIR) cells and thermally treated in vacuum at 120°C and $4 \cdot 10^{-4}$ mbar for one hour before the analysis in order to get the samples clear from etching adsorbed residuals, moisture and possible organic contaminants.

Fourier transform IR characterization was carried out in transmission mode by means of a self-calibrated source spectrometer (Thermo Scientific Nicolet 6700) equipped with a DTGS detector and working with a resolution of 2 cm^{-2}. The instrument optics and the detector cut-off allowed collecting spectra in the 4400-400 cm $^{-1}$ range. Sample A (18 μm) and B (17 μm) were exposed to ethanol and pyridine dosages respectively. After the thermal treatment, the sample cell was connected to a vacuum glass pipeline able to send dosages of

probe molecules in gas phase. The presence of the interference fringes was checked during the sample alignment and beam optimization procedure. This real time check procedure showed the sample to be uniformly transmitting with no strong dependence on the beam position over the sample area. Sample A was exposed to ethanol dosages from 1.5 to 40 mbar, while sample B was exposed from 1.5 to 20 mbar pressure of pyridine. Maximum coverages were reached leaving the cell in equilibrium with the liquid phases of probe molecules until the spectra stabilized. At each dosage, a sequence of spectra was collected following the system evolution until no further changes were observed. The spectra accounted for the present data analysis were the last spectra collected of each sequence. The gas pressure in the line i.e. its dosage, was monitored via a Pirani vacuometer at lower pressures (10^{-4} to 10 mbar range) and an analog membrane barometer for higher pressures (10 to $< 10^2$ mbar range) values. In order to verify the samples response, at qualitative level, at the end of the experiments sample A was exposed to pyridine vapor and sample B to ethanol vapor. It has been previously shown that the electrical charactetistics of these samples are complicated by several concurrent factors, such as the nature of the contacts, Coulomb blockade at the narrower constrictions, and the incomplete formation percolation conductive paths [21, 22]. With IR, on the other hand, only (large) variations of the free carrier concentration are detected.

We exposed the DNN samples to ethanol dosages from 1.5 to 40 mbar and pyridine dosages from 1.5 to 20 mbar. *In situ* infrared spectroscopy (IR) is used to monitor the effect of progressive dosages of both molecules (selected IR spectra are reported in Fig. 1). In the present work, however, we are not interested in a detailed description of the vibrational features, but rather on the evolution of the interference pattern under gas dosage. From the fringe amplitude it is possible to gain insight on the absorption of the material (the imaginary part of the refractive index, k), because fringes disappear in absorbing film. The values obtained are in good agreement with the carrier concentrations extracted by fitting the increase of the IR background absorption to the Drude equation (see Fig. 2), despite the qualitative estimation of k, where surface and interface roughness were not considered. Additionally, using Bragg's relationship for thin films with effective optical thickness $d' = nd$, n being the real part of the refractive index and d the physical thickness of the sample, to label the interference peaks, we can easily extract the value of d', and consequently n. Therefore, with this simple approach, within a single-shot experiment, we can infer the

carrier concentration and the dielectric screening conditions at a given gas dosage.

We have performed density-functional theory calculations (DFT) under the Generalized Gradient Approximation (GGA) using the spin-polarized parametrization of Perdew, Burke and Ernzerhof [23], as implemented in the SIESTA code [24]. We have used a double-ζ polarized basis set for the atomic orbitals of Si, C, N; and a single-ζ orbital for passivating H. Charge densities were described by a plane-wave representation with an energy cutoff of 150 Ry. Calculations were performed on the hydrogen-passivated (111) surface of silicon by applying the supercell approach, using models constituted by slabs with a size of about 25×25 Å in directions parallel to the surface and a thickness of about 15 Å. Lattice parameters in directions parallel to the surface were fixed and values taken from the cleavage of the optimized structure of bulk Si. In all calculations, periodic boundary conditions in three dimensions were applied, with a box size large enough in the direction orthogonal to the surface (around 27 Å) to avoid spurious interactions between periodic images of the system and using the Γ point only. The geometries of all systems were fully relaxed by application of the conjugated gradient algorithm until a forces on individual atoms were less than 0.04 eV/Å.

Constructing a realistic model of the irregular surfaces produced by the electrochemical attack described below is beyond the scope of this work and possibly not within the current computational capabilities if a quantum description of the adsorption chemistry is pursued. Dangling bonds, however, have been shown to be ubiquitous surface and interface defects, even in the cleanest bottom-up grown nanowires [25] and are extremely reactive [26]. In a previous study we have shown that the dangling bond electronic states are relatively independent on the wire growth axis and on the facet where they form [27], thus on the specific local atomic arrangement. In this sense, while certainly oversimplified, our model seems suitable to capture the qualitative features of the adsorption process. Yet, it should be noticed that we cannot exclude that we have overlooked other, more complex bonding configurations, specific of the irregular surface that one expect as a result of the electrochemical process and that molecules that are conformationally more complex than NH_3 could exhibit adsorption mechanisms that are more significantly facet dependent (e.g. at the [100] facet that can in principle provide closely spaced dangling-bond pairs.)

III. RESULTS AND DISCUSSION

Results concerning the evolution of the film optical properties under increasing dosages of ethanol and pyridine are summarized in Fig. 3, where we also include the data collected under a forced condensation step. In the case of ethanol, n is from the start very close to the full saturated value, which occurs at 40 mbar, indicating that pore condensation takes place at relatively low P values (changes for $P > 7.5$ mbar are within 1.5 %). It is right before achieving the full saturation that a drop in the transparency is observed, indicating a sudden activation of charge carriers in the sample. The Si DNN under study has been demonstrated in the past to show noticeable featureless absorption in the IR (Drude absorption) due to free carriers that can be directly injected [16, 27, 28] or de-trapped by reactivation of original dopants [17, 28]. Data reported in Fig. 3 suggest that pore-condensed ethanol is indeed capable of augmenting the concentration of free carriers in the Si skeleton, giving rise to the typical Drude absorption mechanism. The latter yields a reduction of fringe amplitude, i.e. the film loses its transparency. Pyridine, on the contrary, does not reach pore condensation at comparable P values, as confirmed by the monotonic rise of n up to a value of 2. This value is consistent with a composition of 26 % Si (n=3.4) and 74 % condensed pyridine ($n = 1.51$), as expected in the case of a 74 % porosity sample. At reduced P values, however, a very different mechanism, with respect to ethanol, takes place, because absorption is easily observed at quite low dosages of pyridine. This suggests that pyridine is able to increase the free carrier population into the Si skeleton, without any need of reaching condensation.

From the above discussion it appears clear that our two test molecules act in very different ways as charge donors in Si nanowires: while a direct injection mechanism is observed for pyridine, consistently with its reducing character, ethanol can easily reach pore condensation, and free charge generation takes place thereafter. The origin of this charge, if directly injected, or de-trapped through a dielectric screening effect, will be discussed below.

In order to gain more insight in the atomic scale mechanisms leading to an increase in the charge carriers, we have performed first-principles electronic structure calculations based on density-functional theory (DFT) as implemented in the SIESTA code [24]. We have considered the adsorption of pyridine and ethanol at a hydrogen-passivated Si(111) surface, assuming for simplicity that they will be bonded at a Si dangling bond (DB). Pyridine is found to adsorb strongly by forming a covalent bond between the N lone pair and the highly

reactive Si DB (the binding energy, E_b, was found to be 0.62 eV). The bonding mechanism is analogous to that previously reported for NH_3 [27, 28]. Like in that case, a shallow filled molecular state appears some tenths of eV below the conduction band, creating the conditions for a donor-type doping mechanism (see Fig. 4, left panel) [29]. The robustness of a molecular doping scheme that relies on the Si-N interaction is further confirmed by chemisorption of triethylamine, whose electronic structure again features a molecular orbital at energies close to the Si conduction band (not shown here). Analogous behavior is expected for other weak Lewis bases, such as triphenylamine and iso-propylamine. Ethanol binds very loosely to the Si DB (E_b is only 0.29 eV, which is most likely even an overestimate, due to the localized nature of the basis functions [30]) and the Si-O distance is $\sim$ 2.70 Å, to compare with $\sim$ 1.83 Å for the Si-N bond in the case of pyridine. Most importantly, after the adsorption the molecule HOMO is found to lie well inside the band-gap of the host material, without having any effect on the generation of charge carriers (see Fig. 4, right panel). We tested different adsorption configurations, considering the formation of covalent interaction –bonding through O, bonding through H– as well as forcing a physisorbed configuration by placing the molecule at $\sim$ 3.5 Å from a fully H-passivated surface [31]. Similar tests were carried out for other O-based Lewis bases, such as water and acetone, but no qualitative change was observed in any of these cases.

Therefore, the picture that emerges from our results suggests that molecular sensing for the two prototypes of Lewis bases considered relies on fundamentally different mechanisms. Pyridine injects charge in the nanowires in a similar fashion to semiconductor impurity n-type doping: at room temperature an electron of the molecular state can be excited into the Si conduction band, increasing the number of free carriers. This process is robust, because pyridine binds strongly to the most common surface defect and the effect is indeed observed in the IR experiments even at moderate pressures. Ethanol does not inject charge, as indicated by the electronic structure calculations. However, free carrier generation can be accounted for by a screening effect that results in the reactivation of dopants, which are present in large concentrations in the DNN samples. It has been experimentally shown that dielectric confinement effectively deactivates dopants in sub-20 nm stand-alone nanowires [6]. When pore condensation approaches, the dielectric constant of the media surrounding the nanostructured Si increases ($n_{ethanol} = 25$), yielding a great reduction of the effects of dielectric confinement. A simple model based on dielectric mismatch is discussed by Timoshenko

et al. [32] and shows that the activation energy of a boron acceptor decreases from 105 to 30 meV when the media dielectric constant increases from 1 (vacuum) to 25 (ethanol). Similarly, a reduction of phosphorus ionization energy is predicted by Niquet *et al.* [5] when considering the presence of a metallic gate or a high-k dielectric around a stand-alone SiNW. The scenario described is illustrated in the cartoon of Fig. 5.

These considerations have important consequences. (i) Pyridine (or ammonia, or triethylamine) behaves like an n-type dopant, inducing a free carrier concentration that is proportional to the number of molecules that reaches the nanowire surface, i.e. proportional to the pressure (see Fig. 2). (ii) Ethanol (or acetone, or water) can act indirectly as a donor or an acceptor. The nature of the doping –n- vs. p-type– and the carrier concentration depend on the type and concentration of the impurities that are reactivated. Also, no significant dependence on the pressure is expected: when the level of pore condensation is sufficient to de-trap the charge from the deactivated impurities, they will all be reactivated at once and not gradually.

In conclusion, we have reported a paradigmatic case for each of two different carrier generation mechanisms in Si nanowires. By means of a simple analysis of the interference fringes in IR experiments, we have access to the loss of transparency due to charge injection and to the dielectric permittivity of the sample within a single measurement. This approach allowed to outline the different role of direct charge injection and reduced dielectric screening in the molecular doping of Si nanowires.

ACKNOWLEDGMENTS

We acknowledge funding under Contract Nos. 200950I164, TEC2009-06986, FIS2009-12721-C04-03, CSD2007-00041. F.M. greatly acknowledges the Transnational Access Programme of the HPC-EUROPA2 Project No. 228398, with the support of the European Community Research Infrastructure Action of the FP7. Part of this work has been performed at Nanofacility Piemonte, a laboratory supported by Compagnia di San Paolo.

---

[1] R. Rurali, Rev. Mod. Phys. **82**, 427 (2010)

[2] P. V. Radovanovic, Nat. Nanotech. **4**, 282 (2009)

[3] R. Rurali, B. Aradi, T. Frauenheim, and A. Gali, Phys. Rev. B **79**, 115303 (2009)

[4] Y. M. Niquet, L. Genovese, C. Delerue, and T. Deutsch, Phys. Rev. B **81**, 161301 (2010)

[5] M. Diarra, Y.-M. Niquet, C. Delerue, and G. Allan, Phys. Rev. B **75**, 045301 (2007)

[6] M. T. Björk, H. Schmid, J. Knoch, H. Riel, and W. Riess, Nat. Nanotech. **4**, 103 (2009)

[7] M. V. Fernández-Serra, C. Adessi, and X. Blase, Phys. Rev. Lett. **96**, 166805 (2006)

[8] N. Fukata, S. Ishida, S. Yokono, R. Takiguchi, J. Chen, T. Sekiguchi, and K. Murakami, Nano Lett. **11**, 651 (2011)

[9] G. Imamura, T. Kawashima, M. Fujii, C. Nishimura, T. Saitoh, and S. Hayashi, Nano Lett. **8**, 2620 (2008)

[10] D. E. Perea, E. R. Hemesath, E. J. Schwalbach, J. L. Lensch-Falk, P. W. Voorhees, and L. J. Lauhon, Nature Nanotech. **4**, 315 (2009)

[11] J. Ristein, Science **313**, 1057 (2006)

[12] C.-S. Guo, L.-B. Luo, G.-D. Yuan, X.-B. Yang, R.-Q. Zhang, W.-J. Zhang, and S.-T. Lee, Angew. Chem. Int. Edit. **48**, 9896 (2009)

[13] R. Haight, L. Sekaric, A. Afzali, and D. Newns, Nano Lett. **9**, 3165 (2009)

[14] G. D. Yuan, Y. B. Zhou, C. S. Guo, W. J. Zhang, Y. B. Tang, Y. Q. Li, Z. H. Chen, Z. B. He, X. J. Zhang, P. F. Wang, I. Bello, R. Q. Zhang, C. S. Lee, and S. T. Lee, ACS Nano **4**, 3045 (2010)

[15] G. D. Yuan, T. W. Ng, Y. B. Zhou, F. Wang, W. J. Zhang, Y. B. Tang, H. B. Wang, L. B. Luo, P. F. Wang, I. Bello, C. S. Lee, and S. T. Lee, Appl. Phys. Lett. **97**, 153126 (2010)

[16] M. Chiesa, G. Amato, L. Boarino, E. Garrone, F. Geobaldo, and E. Giamello, Angew. Chem. Int. Edit. **42**, 5032 (2003)

[17] E. Garrone, F. Geobaldo, P. Rivolo, G. Amato, L. Boarino, M. Chiesa, E. Giamello, R. Gobetto, P. Ugliengo, and A. Viale, Adv. Mater. **17**, 528 (2005)

[18] M. Beale, J. Benjamin, M. Uren, N. Chew, and A. Cullis, J. Cryst. Growth **73**, 622 (1985)

[19] V. Lehmann and U. Gösele, Appl. Phys. Lett. **58**, 856 (1991)

[20] Canham, L. T., in *Properties of Porous Silicon*, EMIS Data Review Series, Canham, L. T., Editor, **1997**, p. 106, INSPEC, London, UK.

[21] S. Borini, L. Boarino, and G. Amato, Appl. Phys. Lett. **89**, 132111 (2006)

[22] S. Borini, L. Boarino, and G. Amato, Physica E **38**, 197 (2007)

[23] J. P. Perdew, K. Burke, and M. Ernzerhof, Phys. Rev. Lett. **77**, 3865 (1996)

[24] J. M. Soler, E. Artacho, J. D. Gale, A. García, J. Junquera, P. Ordejón, and D. Sánchez-Portal, J. Phys.: Condens. Matter **14**, 2745 (2002)

[25] A. Baumer, M. Stutzmann, M. S. Brandt, F. C. Au, and S. T. Lee, Appl. Phys. Lett. **85**, 943 (2004)

[26] C. R. Leão, A. Fazzio, and A. J. R. da Silva, Nano Lett. **7**, 1172 (2007)

[27] A. Miranda, X. Cartoixà, E. Canadell, and R. Rurali, Nanoscale Res. Lett. **7**, 308 (2012)

[28] A. Miranda-Durán, X. Cartoixá, M. Cruz Irisson, and R. Rurali, Nano Lett. **10**, 3590 (2010)

[29] Activation energies of dopants as calculated within DFT has to be taken qualitatively. The need of a many-body treatment for quantitative estimations of this magnitude is discussed in Ref. [4].

[30] R. Rurali, N. Lorente, and P. Ordejón, Phys. Rev. Lett. **95**, 209601 (2005)

[31] Physisorbed configuration where the molecule binds the surface via a van der Waals interaction are not properly accounted within the local and semi-local formulation of DFT. Hence we froze the molecule at a distance from the surface typical of this kind of weak interactions and we calculated the electronic structure for that geometry.

[32] V. Y. Timoshenko, T. Dittrich, V. Lysenko, M. G. Lisachenko, and F. Koch, Phys. Rev. B **64**, 085314 (2001)

FIG. 1. IR spectra for ethanol and pyridine adsorption. Dashed curves represent the bare DNN, while solid curves correspond to exposed samples. The range is limited at wavenumbers above 1500 cm^{-1} in order to highlight the features of interest: fringes amplitude and step. Bare IR spectra of the samples are characterized, in addition to the interference patterns, by fingerprint at 2100 cm^{-1} of v-SiH formed during the electrochemical etching. In the case of Ehtanol interaction, superimposed to the optical interference features, fingerprint signals of v-CH of CH_2 and CH_3 groups are clearly visible in the range 2990-2830 cm^{-1}, while the broad band centered 3400 cm^{-1} is associated to hydrogen bonded OH groups of ethanol. In case of pyrydine, ring modes around 1599 cm^{-1} and vCH above 3000 cm^{-1} (aromatic ring) are visible.

FIG. 2. Carrier concentrations as a function of gas dosages. The values have been extracted by estimating the increase of the background absorption at large wavelengths (17.5 μm) and fitting them to the Drude equation.

FIG. 3. (a) Refractive index as a function of gas dosages. The values are calculated from the period of the fringes as $n \sim \frac{\lambda_2 \lambda_1}{2d(\lambda_1 - \lambda_1)}$, where λ_1 and λ_2 are the wavelengths of two nearby maxima and d is the sample nominal thickness. (b) Fringes amplitudes (normalized to 1) extracted directly from the spectra plots.

FIG. 4. Adsorption geometry, band structure and projected density of states (PDOS) as obtained by first principles electronic structure calculations for the two systems discussed. Pyridine (left) strongly chemisorbs and provides a shallow state close to the conduction band. The nature of the molecular state is revealed to be essentially an all-N contribution by the PDOS. Ethanol (right) loosely interacts with the Si surface and its HOMO (blue peak) is too deep into the band-gap to be thermally activated. Notice that that the higher β-spin state (red peak) is empty. Si, C, and H atoms are represented with light, cyan, and white spheres respectively. Dark blue and red indicates N and O atoms.

FIG. 5. Cartoon of the different *doping* mechanisms. Pyridine adsorption yields a genuine molecular doping process where one carrier of each adsorbed molecule can be thermally excited into the conduction band of the host material. At sufficiently high pressures, ethanol (right panel) changes the dielectric characteristics of the surrounding medium allowing impurities, otherwise electrically inactive due to dielectric confinement, to be reactivated.

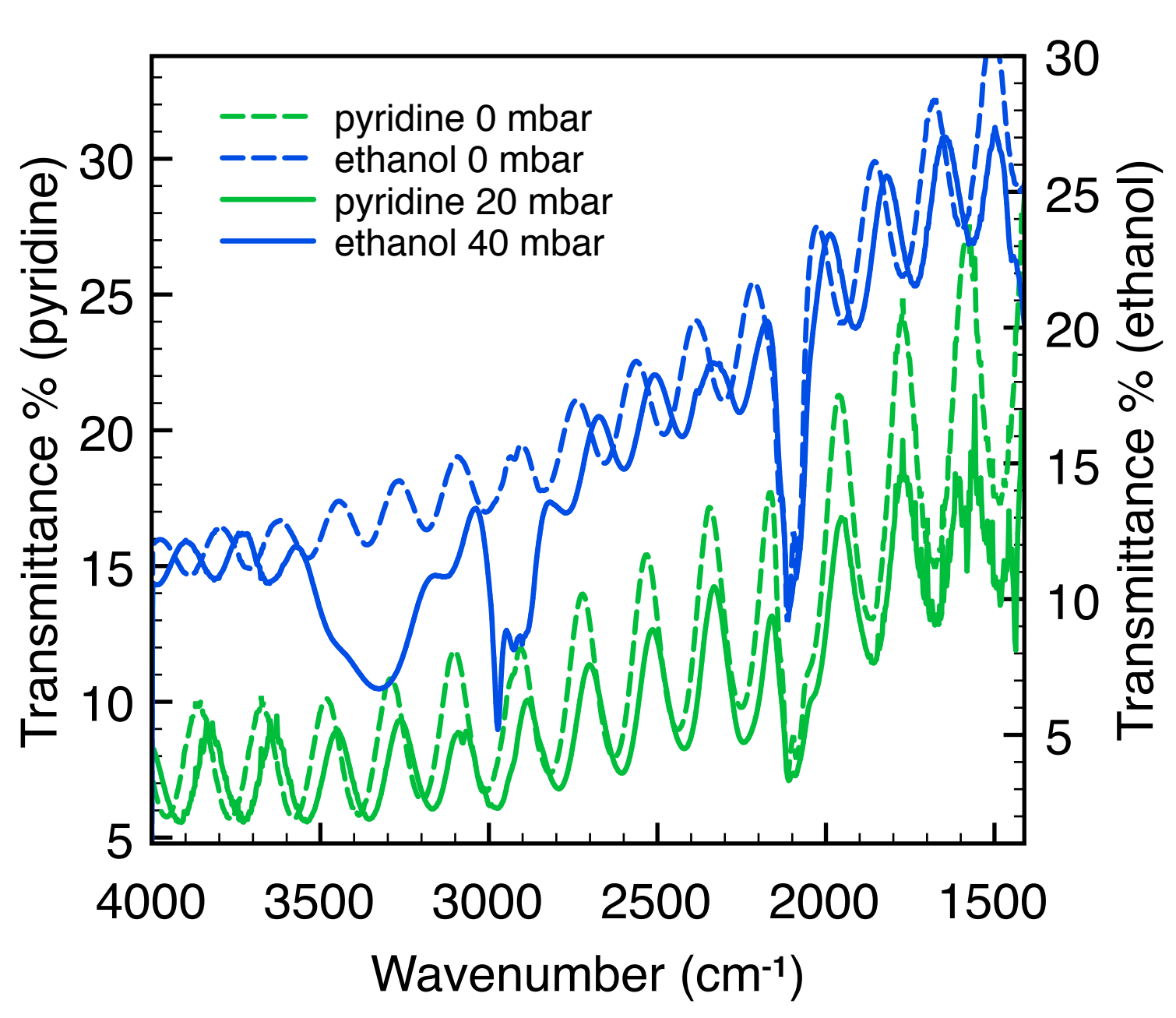
pyridine 0 mbar
ethanol 0 mbar
pyridine 20 mbar
ethanol 40 mbar
Transmittance % (pyridine)
Transmittance % (ethanol)
Wavenumber (cm-1)
4000
3500
3000
2500
2000
1500
30
25
20
15
10
5

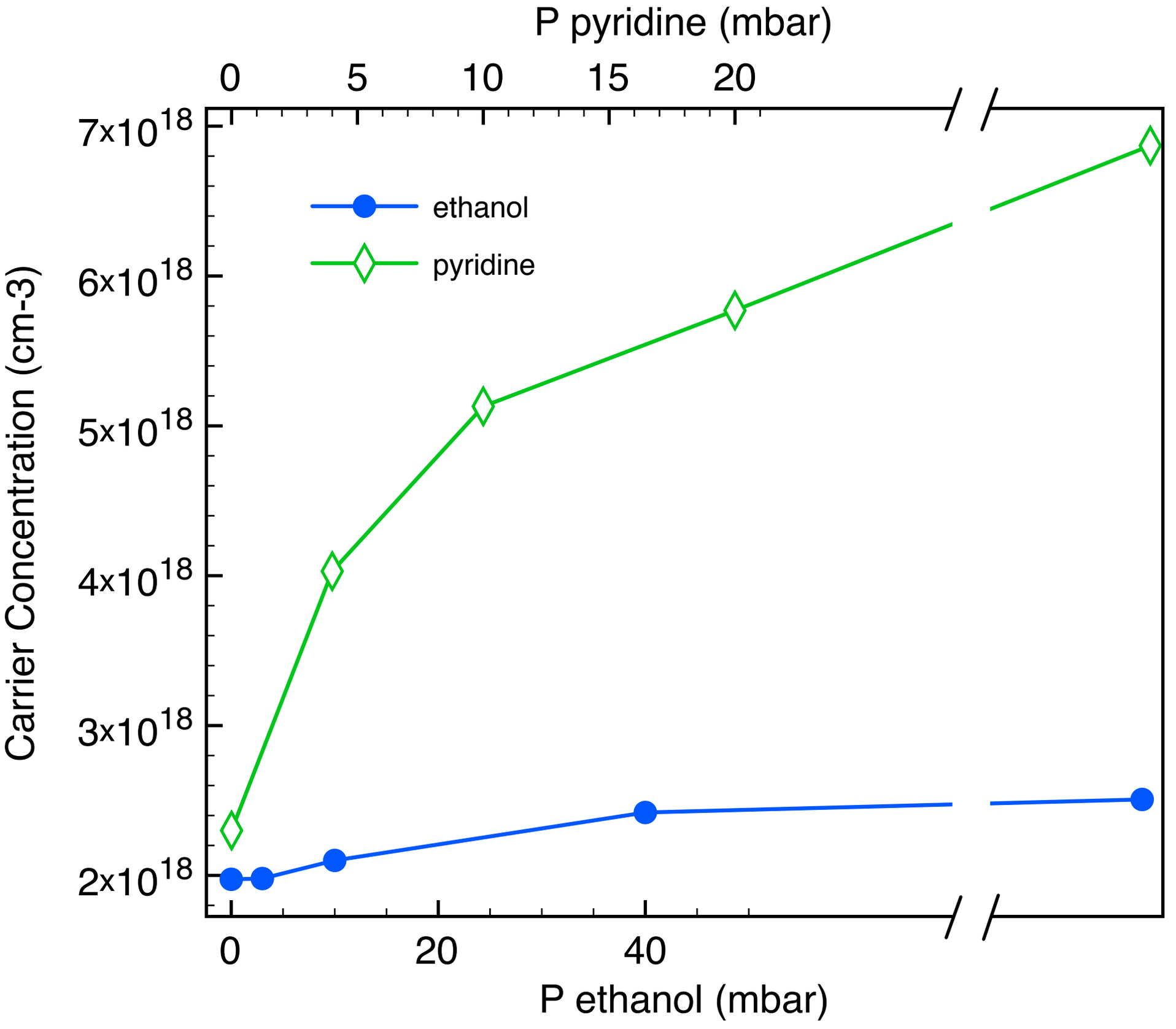
P pyridine (mbar)
0
5
10
15
20
7x10^18
6x10^18
5x10^18
4x10^18
3x10^18
2x10^18
ethanol
pyridine
Carrier Concentration (cm-3)
0
20
40
P ethanol (mbar)

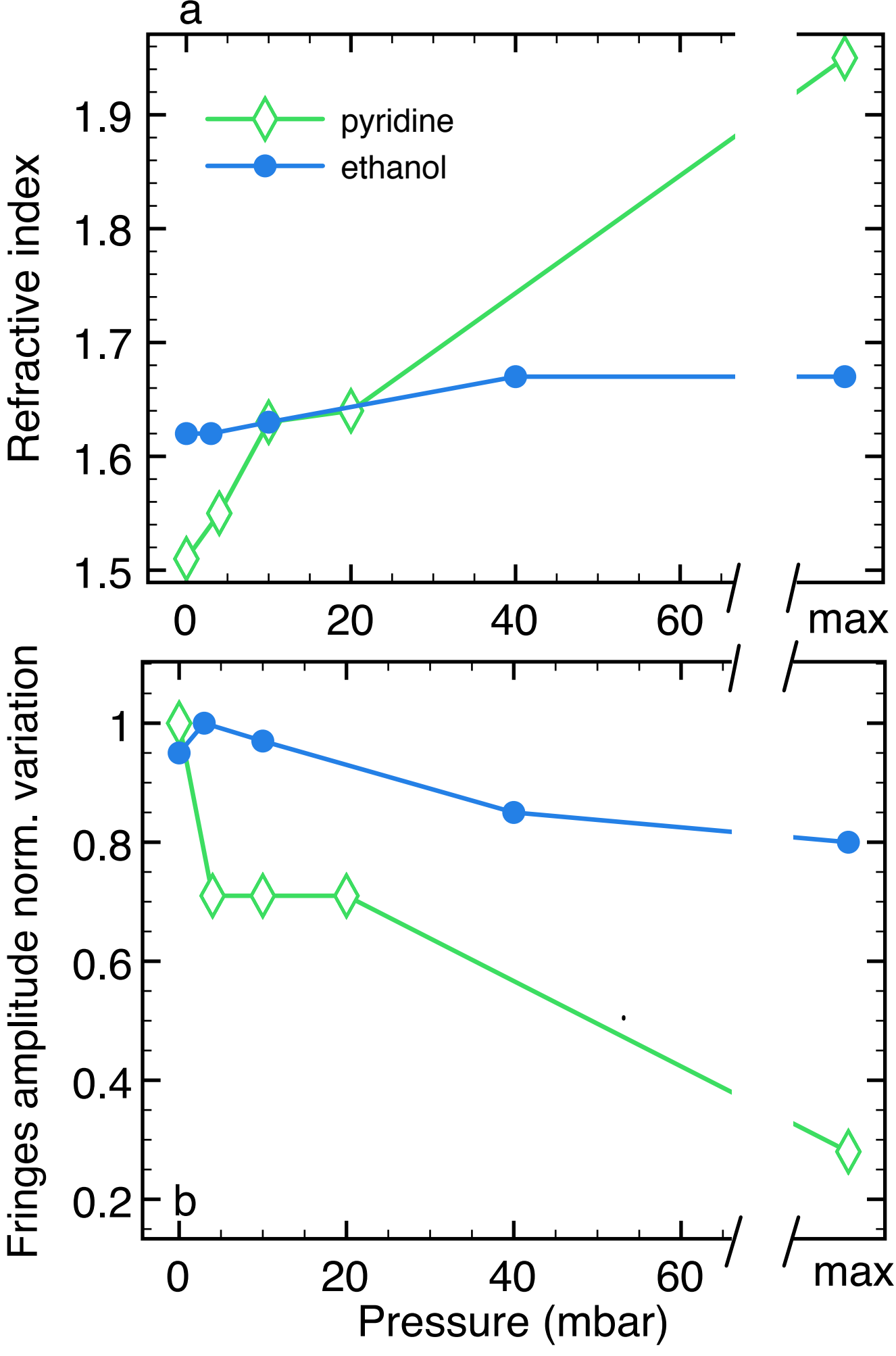
a
Refractive index
1.9
1.8
1.7
1.6
1.5
pyridine
ethanol
0
20
40
60
max
Fringes amplitude norm. variation
1
0.8
0.6
0.4
0.2
b
0
20
40
60
max
Pressure (mbar)

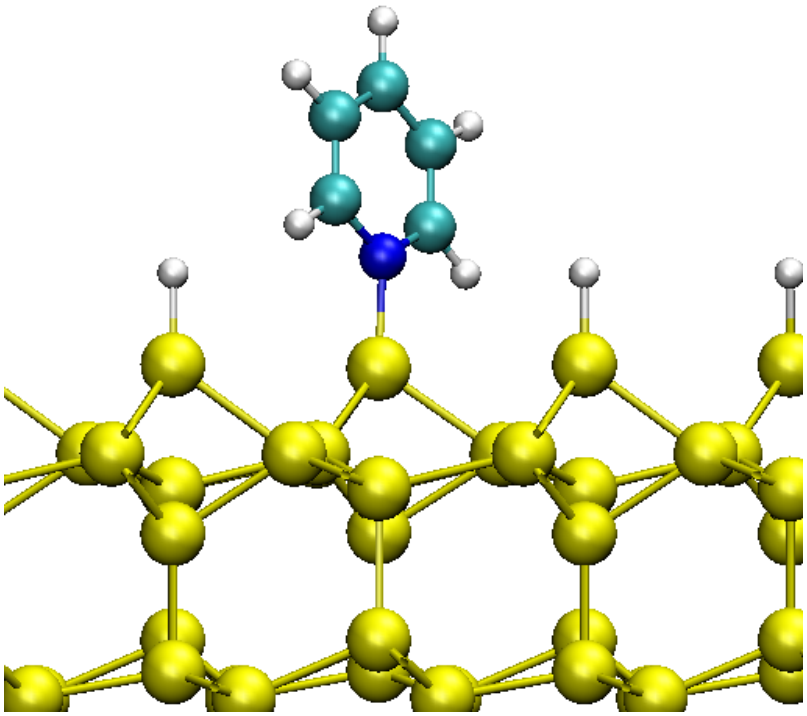

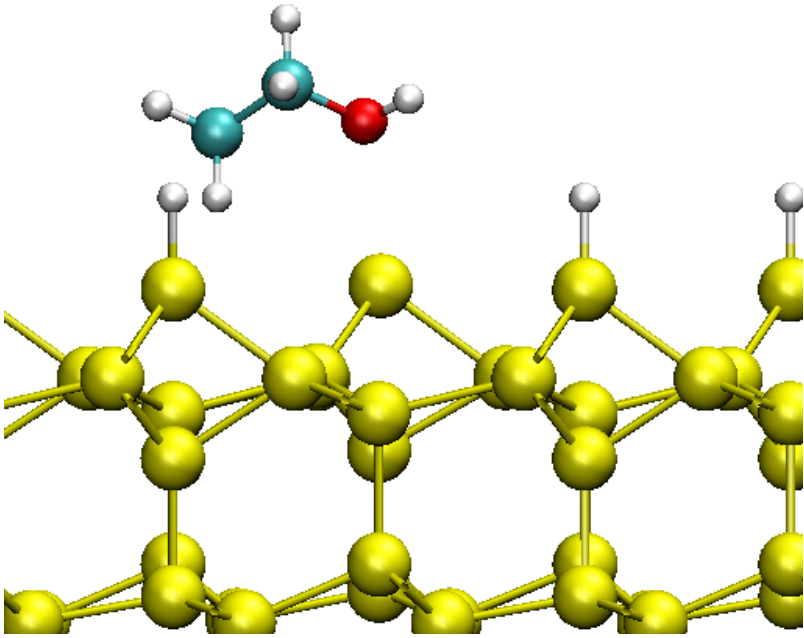

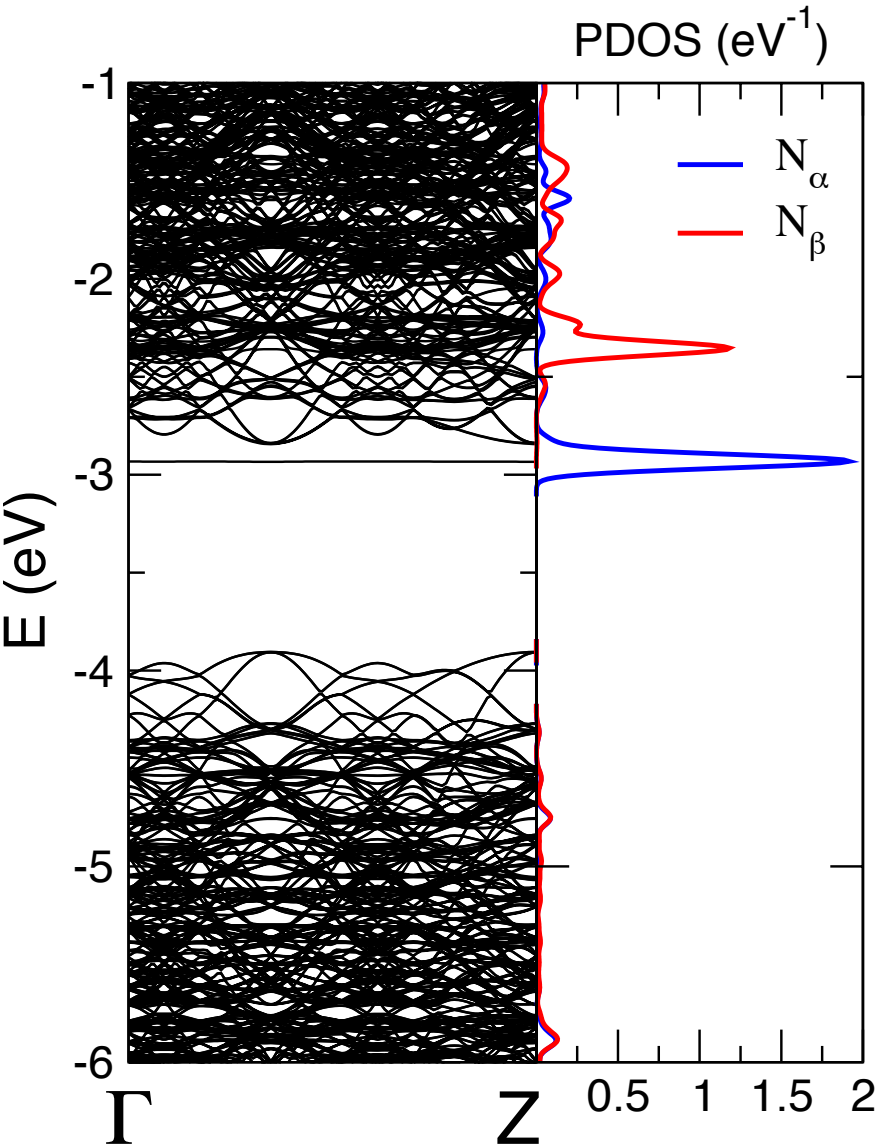
PDOS (eV-1)
-1
-2
-3
-4
-5
-6
E (eV)
Nα
Nβ
Γ
Z
0.5
1
1.5
2

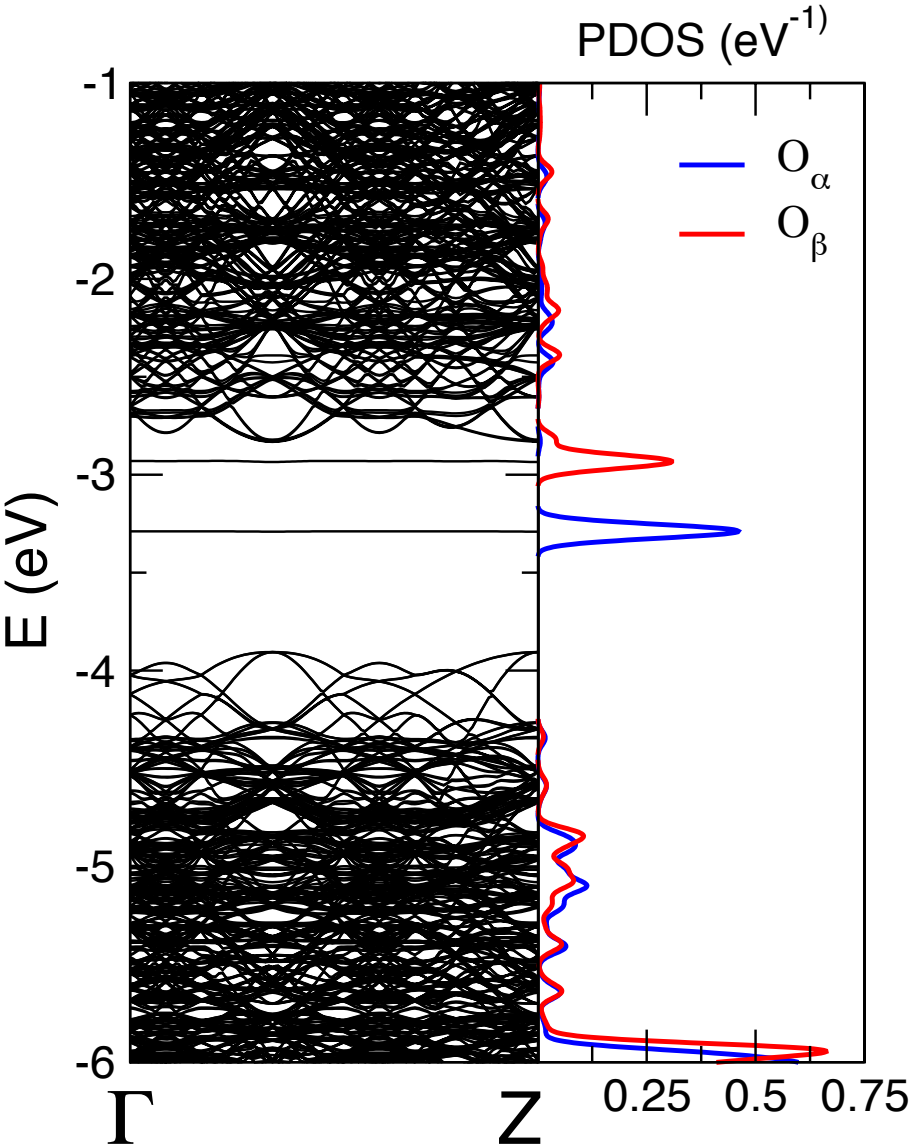
PDOS (eV-1)
-1
-2
-3
-4
-5
-6
E (eV)
Oα
Oβ
Γ
Z
0.25
0.5
0.75

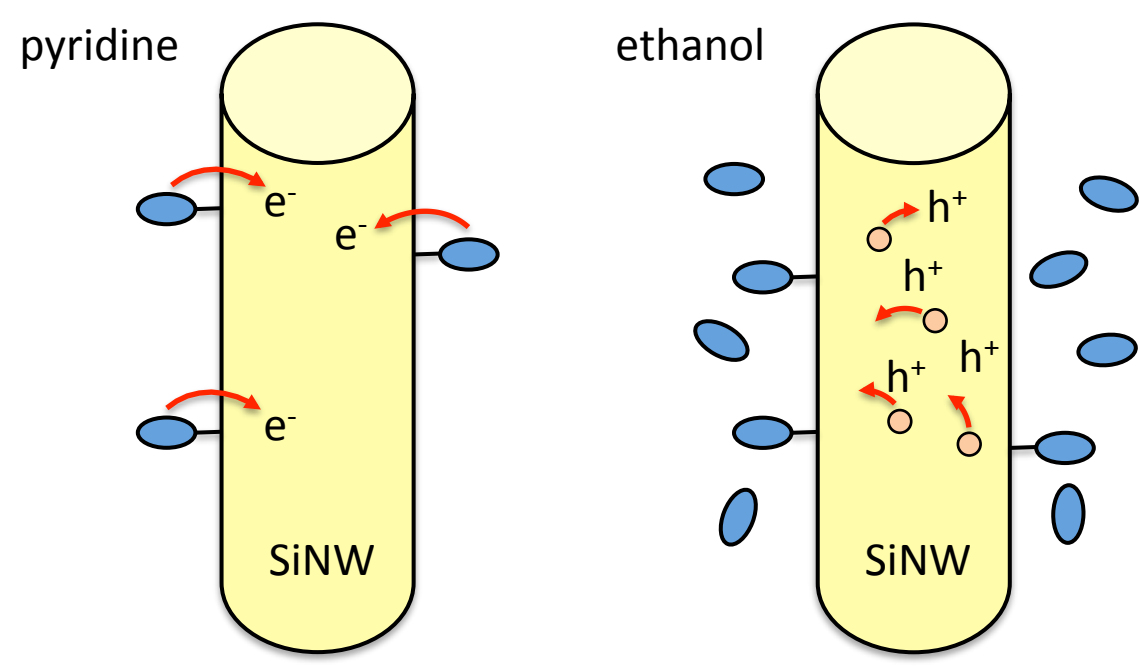
pyridine
e-
e-
e-
SiNW
ethanol
h+
h+
h+
h+
SiNW